

Appendix T—Defining the Inversion Rupture Set Using Plausibility Filters

By Kevin R. Milner,¹ Morgan T. Page,² Edward H. Field,² Tom Parsons,² Glenn P. Biasi,³ and Bruce E. Shaw⁴

Introduction

The Grand Inversion (appendix N, this report) takes as input, among other things, a list of possible ruptures for which it solves for the frequency of occurrence. To relax segmentation, faults from the Uniform California Earthquake Rupture Forecast, version 3 (UCERF3), California Reference Fault Parameter Database (appendix A, this report) are each discretized into equal length subsections with lengths of approximately one-half the seismogenic thickness of the fault. This results in 2,606 subsections for Fault Model 3.1 (FM3.1) and 2,664 subsections for Fault Model 3.2 (FM3.2). Ruptures are then defined as unique lists of these subsections, and are created by stepping through all possible combinations of subsections applying a set of filters to exclude non-physically sensible ruptures. This results in 253,706 ruptures that pass all filtering criteria with 369 of 560 possible junctions included for FM3.1, and 305,709 ruptures with 409 of 607 possible junctions included for FM3.2. A summary of the filtering criteria used in UCERF3, as well as the effect of each filter on the overall rupture count, is given in table T1.

Note that this set of ruptures is an approximation of the system required for tractability of the Grand Inversion. As such, some plausible ruptures are likely excluded, as well as implausible ruptures included. The inversion itself is solely responsible for determining rupture probabilities, with no bearing on the margin with which each rupture passes the thresholds outlined in this appendix.

Maximum Jump Distance

The maximum jump distance criterion specifies the maximum distance in three dimensions between the closest points on each pair of adjacent fault sections in a rupture. Note that in our implementation, for simplicity, ruptures can only jump from one fault section to another fault section at their closest point, provided this distance is within the maximum jump distance these faults can connect. This prevents ruptures from jumping back and forth between two parallel fault sections. Our value of 5 km is consistent with the maximum jump distance in the Wesnousky database of earthquake surface ruptures (Wesnousky, 2008). Rupture and junction counts for various possible distance thresholds are given in table T2. See appendix J (this report) for more discussion of measured rupture-jump statistics.

¹ University of Southern California.

² U.S. Geological Survey.

³ University of Nevada, Reno.

⁴ Columbia University.

Table T1. Summary of Uniform California Earthquake Rupture Forecast, version 3, (UCERF3) rupture criteria.

[“Apply to junctions only” means that the specified criterion is only checked at junctions between two different fault sections, as opposed to every subsection boundary. “Ruptures excluded (FM3.1)” refers to the number of ruptures that would be included in the UCERF3 rupture set for Fault Model 3.1 (FM3.1) if the given filter were disabled (and all other filters were default), or “N/A” if that filter cannot be disabled. Likewise, “Junctions excluded (FM3.1)” refers to the number of junctions that are within the distance threshold but are excluded by the given filter and would otherwise be included. The final UCERF3 rupture set for FM3.1 has 253,706 ruptures with 369 junctions]

Name	Threshold	Apply to junctions only?	Ruptures excluded (FM3.1)	Junctions excluded (FM3.1)
Maximum jump distance	5 kilometer	yes	N/A	N/A
Junction azimuth change	60 degrees	yes	12,909	33
Total azimuth change	60 degrees	no	21,848	3
Cumulative azimuth change	560 degrees	no	> 1,000,000	0
Cumulative rake change	180 degrees	no	13,816	0
Minimum number of subsections per fault	2	no	N/A	N/A
Coulomb filter	$P\Delta CFF \geq 0.04$ or $\Delta CFF \geq 1.25$ bar	yes	258,310	105

Table T2. Rupture counts for various maximum jump distance thresholds for Fault Model 3.1, as well as the number of junctions between different fault sections included by this and other filters, and the total number of possible junctions within the given distance.

[A maximum jump distance of 0 refers to either intersecting faults, or multiple sections of a single fault (such as the San Andreas Fault). The rupture count for 3 km is greater than for 5 km because of a special case in the minimum number of sections per rupture criterion that allows single-subsection connectors if two fault sections cannot otherwise connect (fig. T3). There are fault sections in our rupture set separated by distances between 3 and 5 km that can connect with *multiple* single subsection connectors. In these cases, more ruptures are added to the rupture set if the distance criterion precludes a direct connection between the fault sections. The rupture counts are 243,624 for 5 km and 215,348 for 3 km, if single-subsection connectors are disabled]

Maximum jump distance (km)	Number of ruptures	Number of junctions included	Number of possible junctions
5	253,706	369	560
3	263,880*	334	459
1	171,404	261	321
0.1	38,408	76	84
0	26,021	46	48

Junction Azimuth Change

The junction azimuth change criterion specifies the maximum azimuth change at any jump between different fault sections as defined in the UCERF3 California Reference Fault Parameter Database (henceforward referred to as a junction), regardless of the jump distance. Our value of 60 degrees prevents large changes in rupture strike, such as right angles or U-turns, while allowing ruptures similar to the 2002 Denali earthquake. Although studies such as Xu and Ben-Zion (2013) showed that rupture branching at angles greater than 60 degrees are possible, we determined that increasing the threshold ultimately allows more implausible than plausible ruptures and that our current value is an adequate approximation. Azimuth changes are calculated for this and other criteria by determining the azimuth between the midpoints of the two sections immediately preceding the jump, and comparing it to the azimuth between the midpoints of the two sections immediately following the jump (fig. T1).

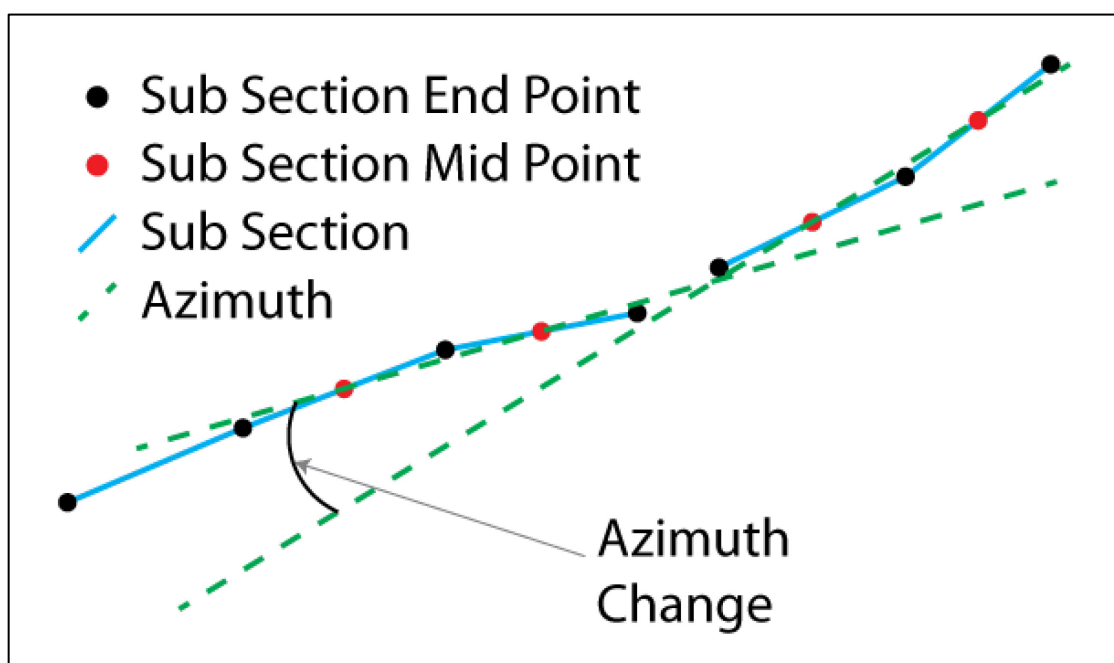


Figure T1. Diagram showing azimuth change calculation methodology. Azimuth changes are calculated by taking the azimuth between the midpoints of the two subsections immediately preceding and following the jump.

A special case is applied for junctions involving certain left-lateral faults, for which we reversed the azimuth of the left-lateral fault to allow, for example, the Garlock Fault to rupture southward with the Mojave section of the San Andreas Fault (and excluding rupture to the north with the Carrizo section). This results in azimuth changes ranging from 120 to 180 degrees and -120 to -180 degrees (and excludes the normally allowed ranges of 0–60 degrees and -60–0 degrees) between left-lateral and non-left-lateral faults. Junctions between two left-lateral faults are required to conform to our regular azimuth change rules. These ruptures, although technically an azimuth change greater than 90 degrees, are preferred for left-lateral faults linking with right-lateral faults by both Coulomb model simulation and earthquake simulators (Richards-Dinger and Dieterich, 2012).

Total Azimuth Change

The total azimuth change criterion specifies the maximum azimuth change between the start and end of the rupture. This prevents ruptures from forming circles or direction reversal where each individual junction still passes the junction azimuth change filter. If either the first or last sections of the rupture are left-lateral, the azimuths are reversed as described in section, “Junction Azimuth Change.” This filter is only applied to ruptures with at least one junction.

Cumulative Azimuth Change

The cumulative azimuth change criterion, known colloquially as the “squirrelly-ness” filter, prevents ruptures that move back and forth many times by summing the absolute value of the azimuth change between each subsection in the rupture. This filter is needed in the UCERF3 fault models because of the high density of faults that could otherwise link in the Ventura and Los Angeles basins. An example of the type of rupture excluded by this filter is shown in figure T2. Without this filter, the number of ruptures would reach hundreds of millions and the inversion would be computationally intractable. Increasing the maximum cumulative azimuth change significantly increases the number of ruptures; the current value of 560 degrees is set to keep the number of ruptures low while being high enough to allow near “wall-to-wall” San Andreas ruptures.

Cumulative Rake Change

The cumulative rake change criterion limits the sum of absolute values of rake changes within a rupture. This prevents many fault sections with different rakes from linking up in an individual rupture. The value of 180 degrees, for example, allows right-lateral faults to connect with left-lateral faults or normal faults to connect with reverse faults a single time in a given rupture. It disallows multiple, large rake changes, for example, right lateral—left lateral—right lateral. Rakes from the geologic deformation model are always used for filtration to maintain a consistent set of ruptures for each deformation model.

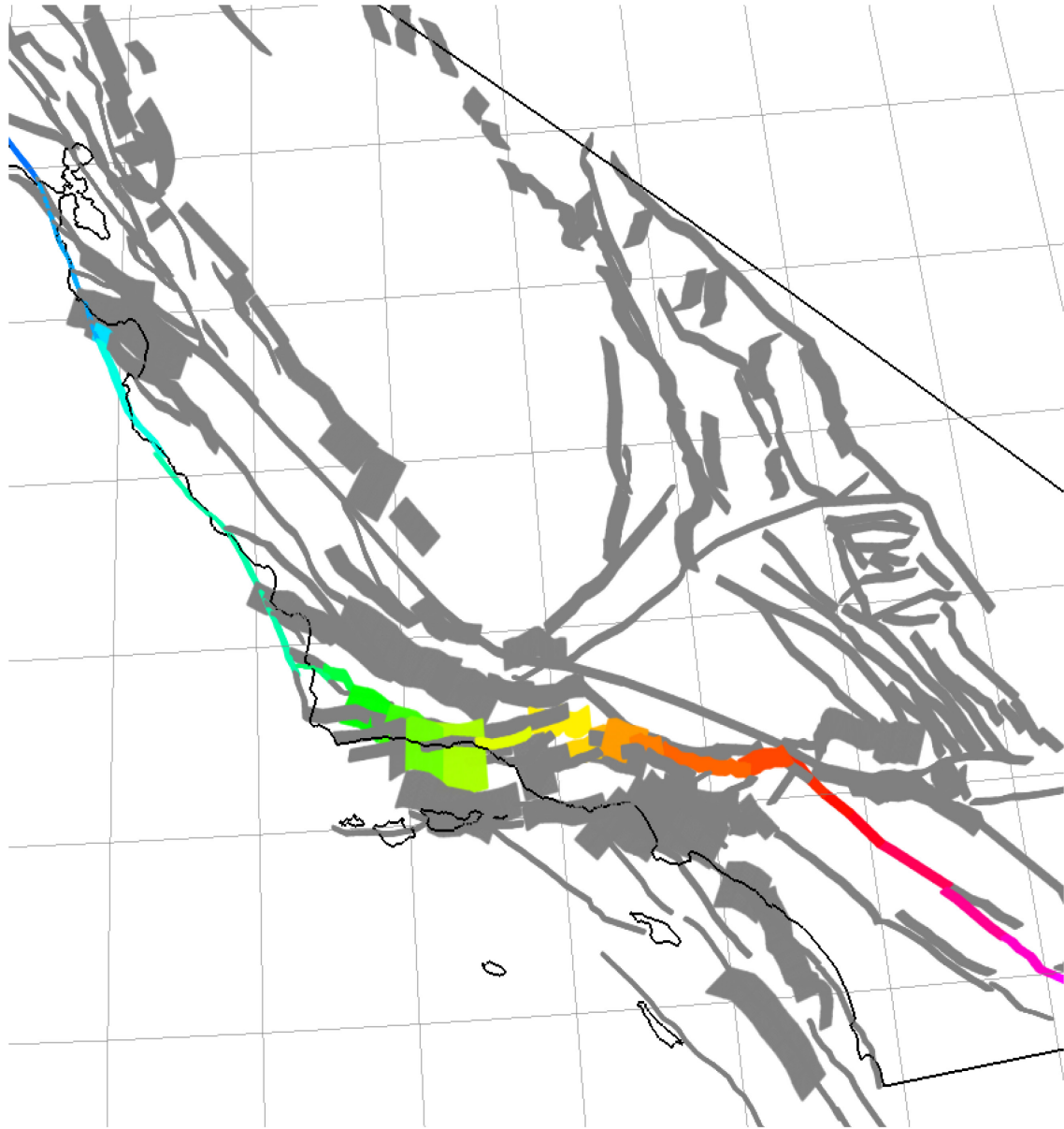


Figure T2. Illustration showing an example rupture that is excluded by the cumulative azimuth change filter. Each color represents a unique fault section.

Minimum Number of Subsections per Fault

At least two subsections are required from each fault involved in a given rupture. This is required for our azimuth change filters, and this requirement also prevents ruptures that jump onto a fault section for a single subsection before continuing on the main fault. An exception to this rule is made where two faults can only connect by jumping onto a single fault section of another fault. This can be caused by a segment boundary immediately next to a junction (fig. T3). Azimuth changes for all azimuth filters are computed by using the midpoints of the single connector subsection as well as the first subsection of the next fault.

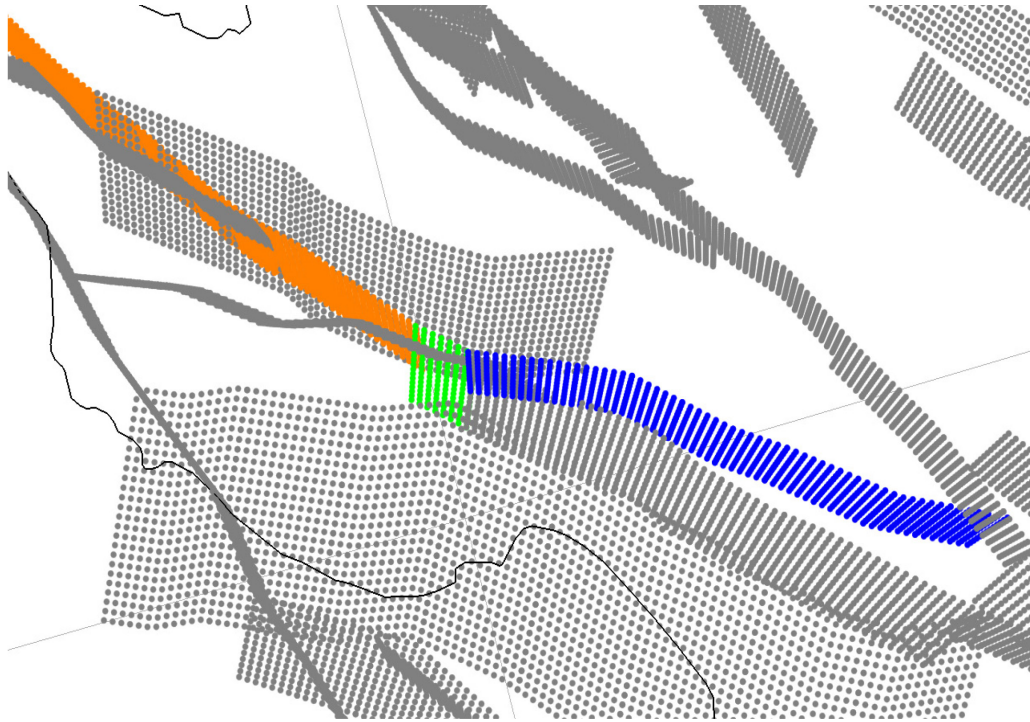


Figure T3. Illustration showing where the Sargent Fault (blue) can only connect with the Peninsula section of the San Andreas Fault (orange) by including a single section of the Santa Cruz Mountains section (green). This is allowed by a special exception to the minimum number of sections per fault filter.

Coulomb Filter

The Coulomb filter criterion checks the Coulomb compatibility of subsections involved in each rupture junction. Parsons and others (2012) outline the methodology for computing Coulomb failure stress change (ΔCFF) between each pair of subsections within the maximum rupture jump distance of 5 km. Each subsection is broken down into 1×1 -km dislocations, to depict complex geometries, and assigned a uniform slip of 0.1 m (required to establish a relative ranking for each junction). Geologic rakes are used for all ΔCFF calculations to ensure a constant rupture set across all deformation models. ΔCFF for each pair of subsections is then defined as the maximum ΔCFF using each dislocation as a source:

$$\Delta CFF \equiv |\Delta\tau_f| + \mu(\Delta\sigma_n - \Delta p) \quad (T1)$$

where $\Delta\tau_f$ is the change in shear stress on the receiver subsection, μ is the coefficient of friction (we use a constant $\mu = 0.5$), and Δp is the pore pressure change (neglected for this study). ΔCFF is not symmetric ($\Delta CFF_{i,j} \neq \Delta CFF_{j,i}$) and is computed in both directions.

We then define the relative Coulomb favorability ratio $PACFF_{i,j}$ for each subsection s_i to a subsection s_j within 5 km, as the ratio of $\Delta CFF_{i,j}$ to the sum of the n ΔCFF values of each subsection s_k within 5 km of s_i :

$$PACFF_{i,j} = \Delta CFF_{i,j} / \sum_{k=1}^{k=n} (\Delta CFF_{i,k}) \quad (T2)$$

See figure T4 for an illustration of this calculation for a case where three fault sections connect. $PACFF$ provides a useful means for filtering less favorable subsection connections, and

we required that $P\Delta CFF \geq 0.04$ at each junction in a rupture. One shortcoming of this $P\Delta CFF$ threshold is the sensitivity to the number of possible connections (with many possible connections resulting in lower $P\Delta CFF$ values for each individual connection) and outliers (where one very large ΔCFF value reduces $P\Delta CFF$ of each other connection). These shortcomings are addressed by allowing junctions less than the $P\Delta CFF$ threshold but have a $\Delta CFF \geq 1.25$ bar. Additionally, because each subsection pair has $P\Delta CFF$ and ΔCFF values for each direction, we only included ruptures which pass the test in at least one possible rupture propagation direction, including the possibility of nucleation between two junctions and propagating outward, as shown in figure T5. Examples of ruptures allowed by the previous filters but excluded by the Coulomb filter are shown in figure T6.

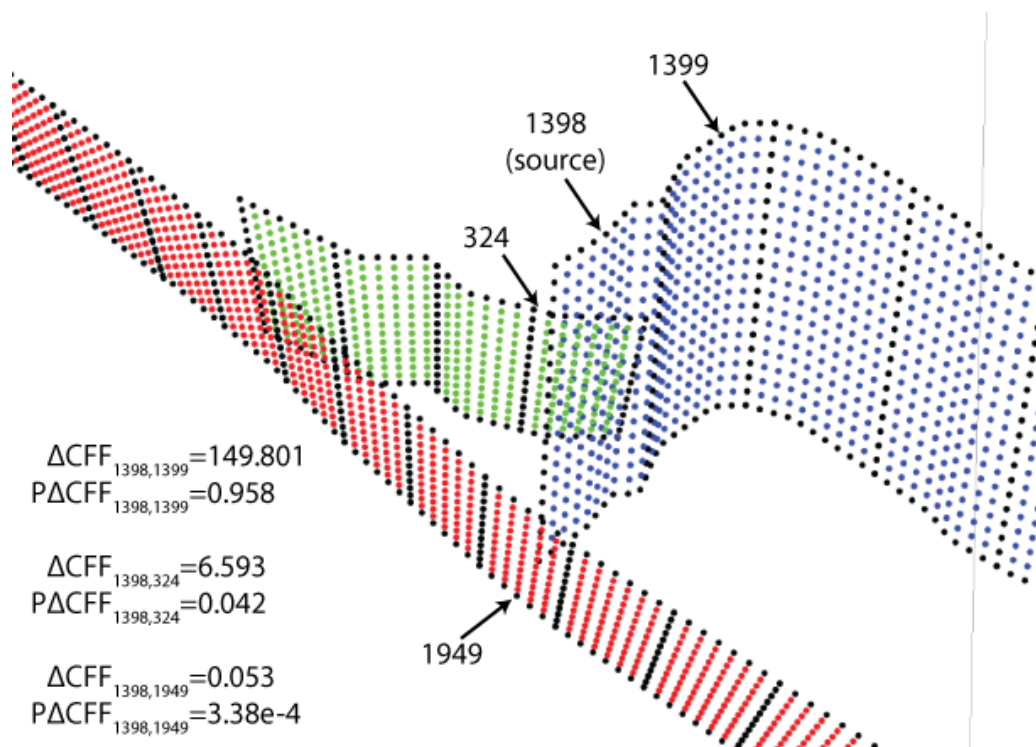


Figure T4. Coulomb favorability ratio ($P\Delta CFF$) illustration showing ruptures jumping from the North Frontal (subsection 1398, rake=90 degrees) to the Cleghorn (subsection 324, rake=0 degrees) and San Andreas (San Bernardino North, subsection 1949, rake=180 degrees). In this case, receiving subsection 1399 is exceptionally well aligned to receive Coulomb stress from a unit slip on 1398. More typical strike-slip subsections connect to their adjacent subsections with 6–15 bars. The sum of all Coulomb failure stress change (ΔCFF) values are 156.447 bar, so $P\Delta CFF_{1398,j} = \Delta CFF_{1398,j} / 156.447$, (for example, the junction from subsection 1398–324, $P\Delta CFF_{1398,324} = \Delta CFF_{1398,324} / 156.447 = 6.593 / 156.447 = 0.042$). In this case, the North Frontal Fault can connect with the Cleghorn Fault because $P\Delta CFF \geq 0.04$. If the $P\Delta CFF$ threshold were more strict, the junction would still be included as $\Delta CFF \geq 1.25$. However, the North Frontal Fault cannot connect with the San Andreas Fault as it violates the $P\Delta CFF$ and ΔCFF thresholds.

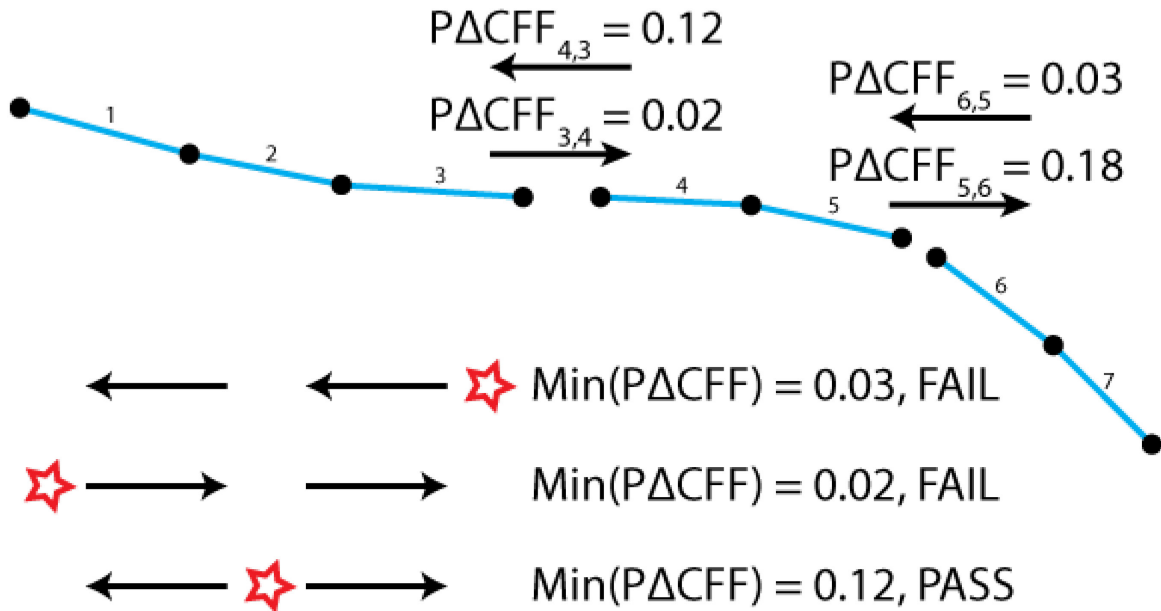


Figure T5. Illustration showing a Coulomb filter example for a rupture with two junctions. In this example (with a Coulomb favorability ratio threshold of 0.04), the rupture passes the case where the hypocenter is on the middle fault section and is included in the set of possible ruptures. No priority is given to ruptures which pass in multiple propagation directions; if a rupture passes in any nucleation case, it is included in the rupture set.

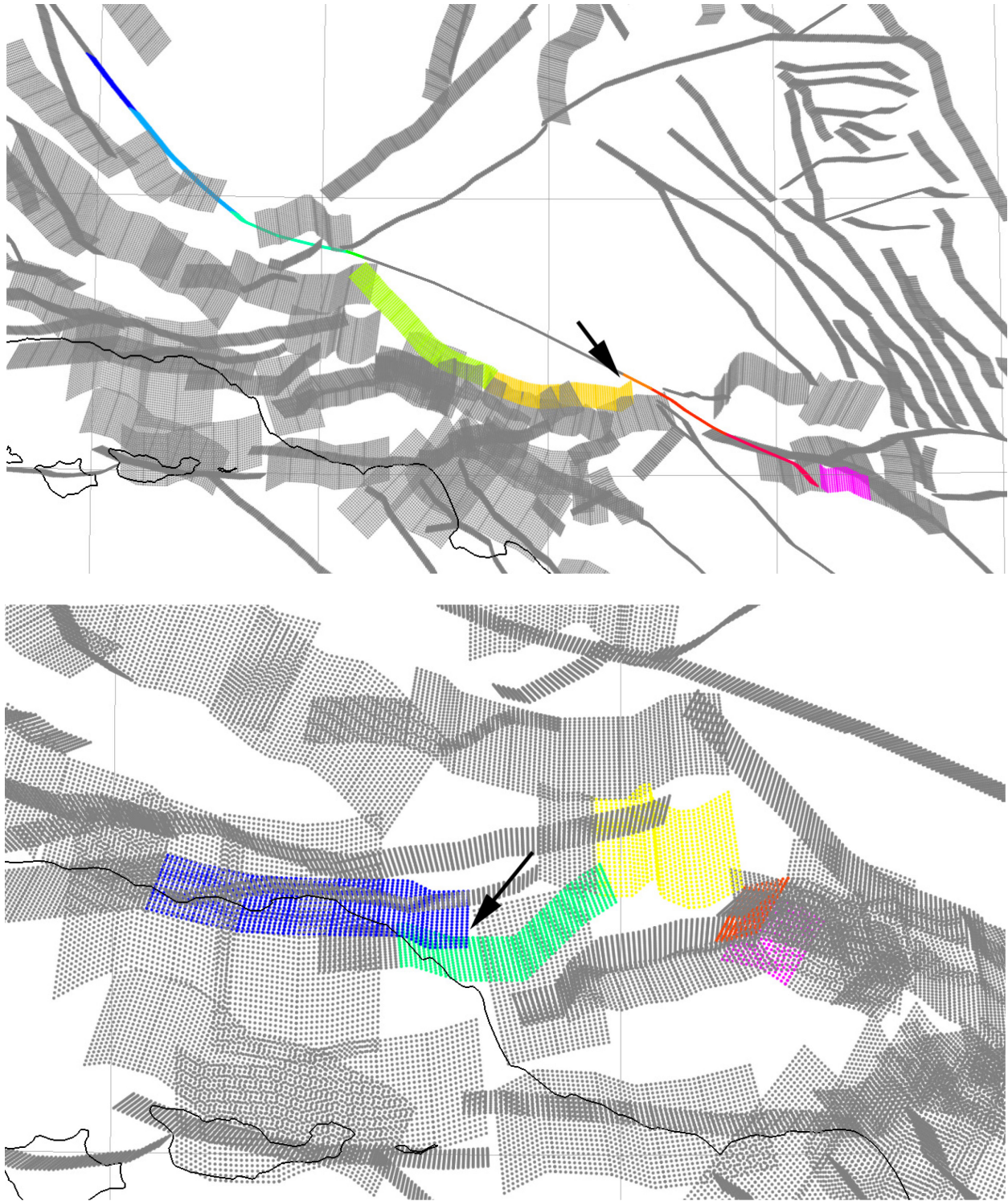


Figure T6. Illustration showing example ruptures excluded by the Coulomb filter that would otherwise be included. Each color represents a different fault section (fault sections not involved in the rupture are gray). The junction that fails the Coulomb test is highlighted with a black arrow.

Table T3. Number of ruptures and junctions excluded by the Coulomb filter from the set of all ruptures that pass all other filters for a variety of Coulomb favorability ratio ($P\Delta CFF$) and Coulomb failure stress change (ΔCFF) threshold values. Currently used thresholds are highlighted with bold text.

$P\Delta CFF$	ΔCFF (bar)	Number of ruptures excluded	Number of junctions excluded
0.02	1.0	117,580	55
0.02	1.25	119,278	57
0.02	1.5	119,727	58
0.02	(off)	141,327	59
0.04	1.0	256,305	102
0.04	1.25	258,310	105
0.04	1.5	259,868	107
0.04	(off)	266,885	110
0.06	1.0	287,618	134
0.06	1.25	300,317	140
0.06	1.5	308,132	146
0.06	(off)	317,470	159
0.08	1.0	293,716	148
0.08	1.25	312,393	156
0.08	1.5	323,376	164
0.08	(off)	345,929	185
0.1	1.0	300,194	152
0.1	1.25	319,295	163
0.1	1.5	330,738	173
0.1	(off)	357,339	200

The cutoff parameters used in the Coulomb filter (table T3, shown in bold,) were chosen because they define a minimal rupture set that allows all of the probable fault section connections, identified at the UCERF fault-by-fault evaluation. Examples of ruptures allowed by this set of parameters (but excluded by more stringent Coulomb parameters) are shown in figure T7.

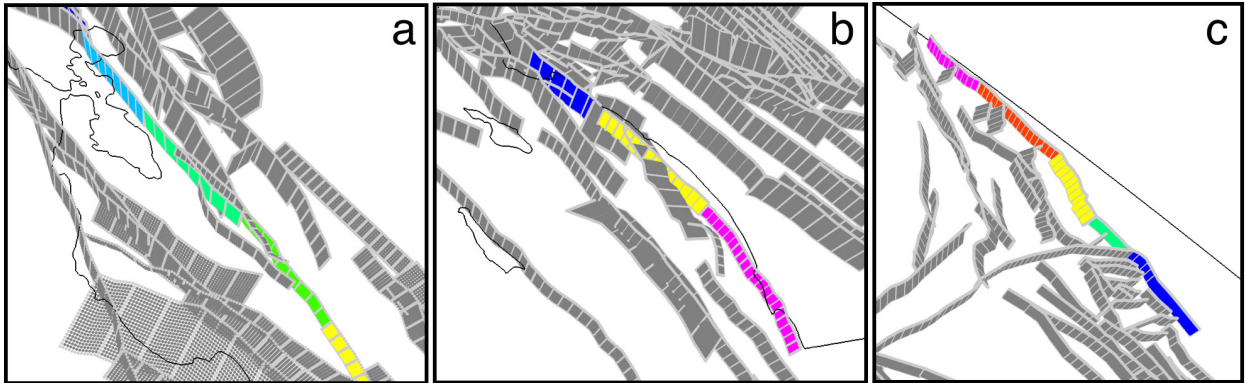


Figure T7. Illustration showing example ruptures included by the Coulomb filter; Coulomb filter parameters were chosen to include junctions such as (a) Hayward Fault to Calaveras Fault, (b) Newport-Inglewood Fault, and (c) Death Valley Fault to Baker Fault.

Characteristics of the Final Rupture Set

The set of ruptures that satisfies all of the criteria previously mentioned is used as input to the Grand Inversion that solves for the rate of each rupture. One side effect of the subsection discretization is that the majority of the ruptures are very long. A histogram of rupture lengths both as discretized (before inversion) and convolved with the UCERF3 rupture rates is shown in figure T8. Figure T9 shows all fault sections that rupture with the Coachella section of the San Andreas Fault after applying the previously mentioned rules. This shows how the Grand Inversion reduces the rate of long and multi-fault ruptures relative to their frequency in the initial rupture set. In particular, figure T9 shows that slip-rate differences between faults strongly control the rate of multi-fault ruptures, as indicated in the inversion-modified rates of ruptures connecting the San Andreas Fault to secondary faults with lower slip rates.

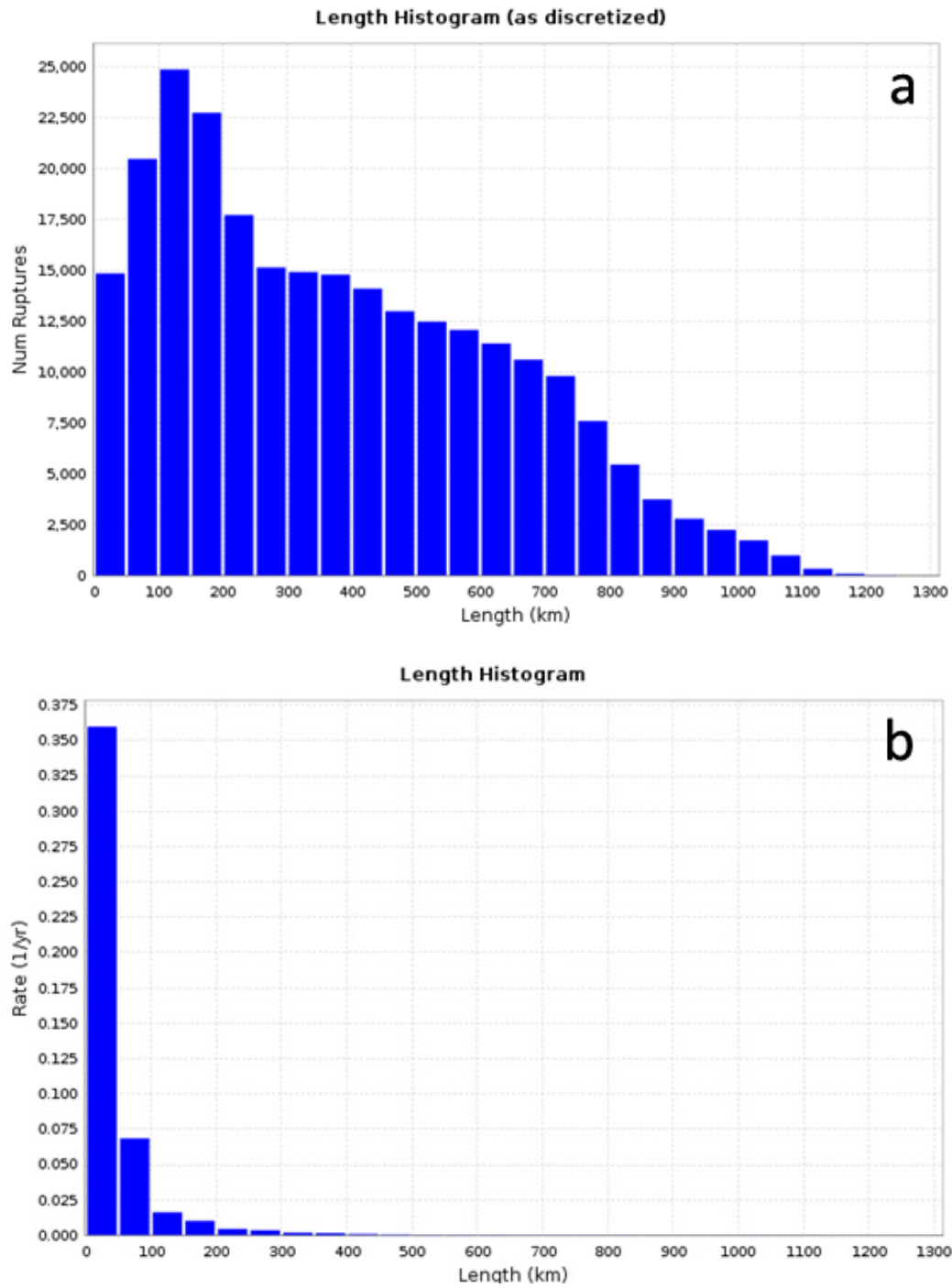


Figure T8. Rupture length histograms for Uniform California Earthquake Rupture Forecast, version 3, (UCERF3) Fault Model, version 3.1 (FM3.1). (a) shows the distribution of lengths as discretized in the uninverted rupture set (with equal weight assigned to each rupture as opposed to post-inversion rupture rates). (b) shows the total rate of each rupture in each length bin for the UCERF3 model.

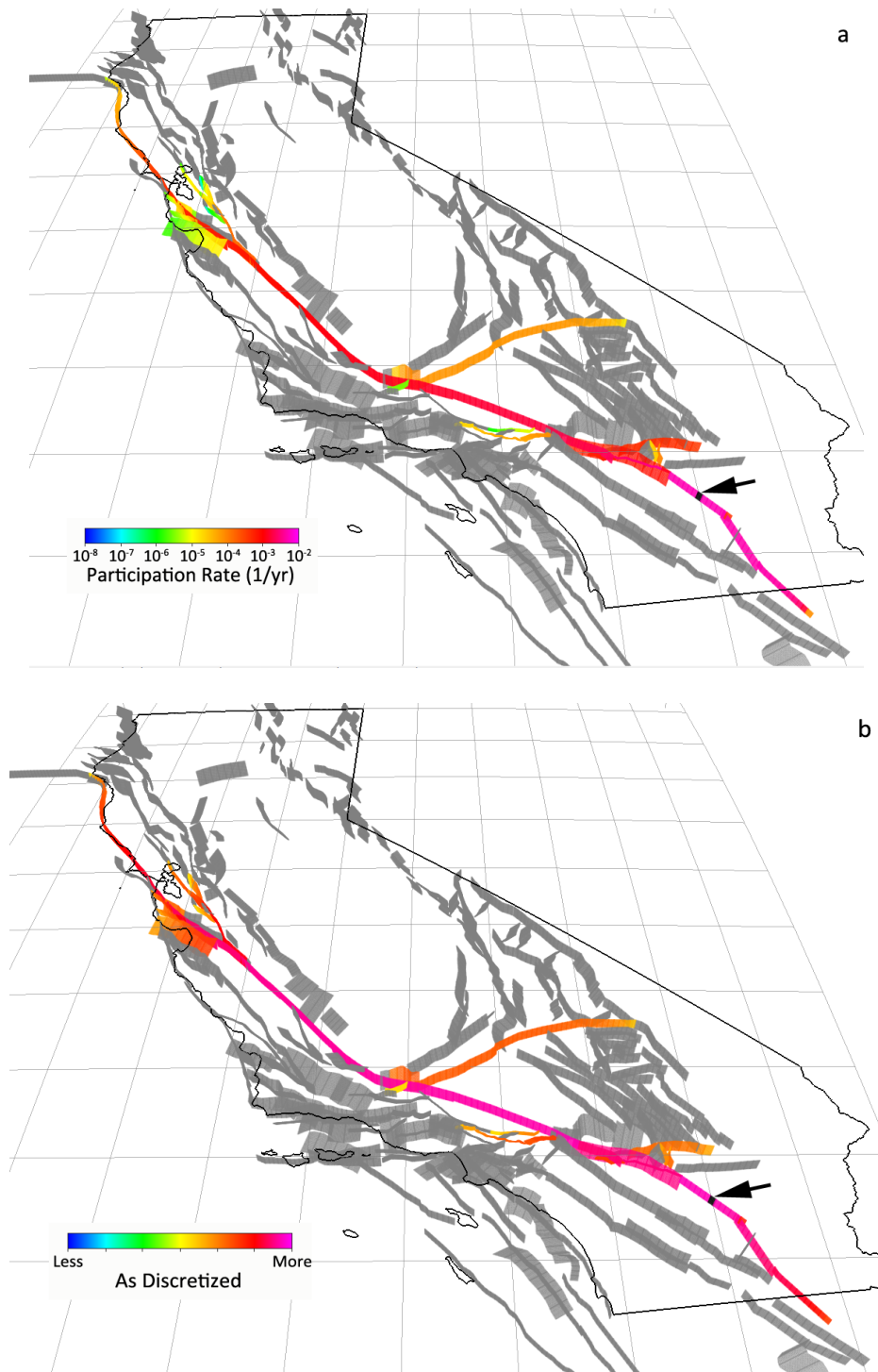


Figure T9. Illustrations showing the number and rates of ruptures which involve a subsection on the Coachella section of the San Andreas Fault (highlighted in black and with an arrow) for Uniform California Earthquake Rupture Forecast, version 3, (UCERF3) Fault Model, version 3.1 (FM3.1). Each subsection in (a) is colored according to the number of ruptures it participates in, including the highlighted Coachella subsection, showing the discretization of the uninverted set. (b) shows the rate at which each subsection participates with the highlighted Coachella subsection for the UCERF3 model.

References Cited

- Parsons, T., Field, E.H., Page, M.T., and Milner, K., 2012, Possible earthquake rupture connections on mapped California faults ranked by calculated coulomb linking stresses: *Bulletin of the Seismological Society of America*, v. 102, no. 6, p. 2667–2676, doi:10.1785/0120110349.
- Richards-Dinger, K., and Dieterich, J.H., 2012, RSQSim earthquake simulator: *Seismological Research Letters*, v. 83, no. 6, p. 983–990. doi:10.1785/0220120105.
- Wesnousky, S.G., 2008, Displacement and geometrical characteristics of earthquake surface ruptures—Issues and implications for seismic-hazard analysis and the process of earthquake rupture: *Bulletin of the Seismological Society of America*, v. 98, no. 4, p. 1609–1632, doi:10.1785/0120070111.
- Xu, S., and Ben-Zion, Y., 2013, Numerical and theoretical analysis of in-plane dynamic rupture on a frictional interface and off-fault yielding patterns at different scales: *Geophysical Journal International*, v. 193, no. 1, p. 304–320.